Geophysical Research Letters

Key Points:
- The role of solar forcing in global warning is unclear due to the uncertainty in the change in TSI since the Maunder minimum
- The TSI level of the Sun when it is in its least-active state is established from an advanced model of TSI variability
- This lower limit on grand minima TSI truncates the current range of the possible change in TSI since the Maunder minimum by more than half

Supporting Information:
- Supporting Information S1

Correspondence to:
K. L. Yeo,
yeo@mps.mpg.de

The Dimmest State of the Sun

K. L. Yeo[1] , **S. K. Solanki[1,2]** , **N. A. Krivova[1]** , **M. Rempel[3]** , **L. S. Anusha[1]** , **A. I. Shapiro[1]** , **R. V. Tagirov[1,4]** , **and V. Witzke[1]**

[1]Max Planck Institute for Solar System Research, Göttingen, Germany, [2]School of Space Research, Kyung Hee University, Yongin, South Korea, [3]High Altitude Observatory, National Center for Atmospheric Research, Boulder CO, USA, [4]Blackett Laboratory, Imperial College London, London, UK

Abstract How the solar electromagnetic energy entering the Earth′s atmosphere varied since preindustrial times is an important consideration in the climate change debate. Detrimental to this debate, estimates of the change in total solar irradiance (TSI) since the Maunder minimum, an extended period of weak solar activity preceding the industrial revolution, differ markedly, ranging from a drop of $0.75 \, \mathrm{W \, m^{-2}}$ to a rise of $6.3 \, \mathrm{W \, m^{-2}}$. Consequently, the exact contribution by solar forcing to the rise in global temperatures over the past centuries remains inconclusive. Adopting a novel approach based on state-of-the-art solar imagery and numerical simulations, we establish the TSI level of the Sun when it is in its least-active state to be $2.0 \pm 0.7 \, \mathrm{W \, m^{-2}}$ below the 2019 level. This means TSI could not have risen since the Maunder minimum by more than this amount, thus restricting the possible role of solar forcing in global warming.

Plain Language Summary How the amount of energy the Earth receives from the Sun varied since preindustrial times is an important consideration in the climate change debate. Detrimental to this debate, it is not known whether the Sun grew brighter or dimmer since the 16th century, and by how much. As a consequence, the exact contribution by fluctuations in the brightness of the Sun to the rise in global temperatures over the past centuries remains controversial. It is established that the Sun was particularly inactive over much of the 16th century. Adopting a novel approach based on state-of-the-art solar imagery and computer models, we determined the brightness of the Sun when it is in its least-active state possible. This places a strict limit on how much the Sun could have grown brighter since the lull in solar activity over the 16th century, restricting the possible role the Sun could have played in global warming.

1. Introduction

Climate change is one of the most pressing challenges facing humanity. The urgency is underscored by the recent pronouncement by the Intergovernmental Panel on Climate Change that greenhouse gas emissions will have to be halved by 2030 to keep global warming below the critical threshold of 1.5° C (IPCC, 2018). Numerical simulations of the Earth′s climate are central to the understanding of past climate and predictions of future trends. They require, as input, the time variation in the various agents of climate change, both anthropogenic and natural (IPCC, 2013). A key natural driver is the variability in the electromagnetic energy reaching the Earth from the Sun (Gray et al., 2010). This is usually described in terms of solar irradiance, which is the solar radiative flux above the Earth′s atmosphere at the mean Earth-Sun distance. The long-term or secular trend in solar irradiance since preindustrial times and how this variability is distributed in wavelength are of particular interest for their relevance to the overall influence of the Sun on the Earth′s climate over the past centuries (Solanki et al., 2013). In this article, our focus will be on the particular issue that current estimates of the secular change in the wavelength-integrated total solar irradiance (TSI) since the 16th century diverge significantly, ranging from a drop of $0.75 \, \mathrm{W \, m^{-2}}$ to a rise of $6.3 \, \mathrm{W \, m^{-2}}$ (Coddington et al., 2016; Dasi-Espuig et al., 2016; Egorova et al., 2018; Judge et al., 2012; Lockwood & Ball, 2020; Schrijver et al., 2011; Shapiro et al., 2011; Steinhilber et al., 2009; Tapping et al., 2007; Wu et al., 2018).

Since the reliable measurement of solar irradiance only started in 1978 (Kopp, 2014), climate simulations rely on models of solar irradiance variability to provide the requisite historical solar forcing input. Except at

the shortest and the longest time scales, where oscillations, convection, and stellar evolution become relevant, solar activity is dominated by its magnetism, making it the prime candidate driver of solar irradiance variability at intermediate time scales (Solanki et al., 2013). Indeed, various studies have demonstrated the variation in solar irradiance at time scales of days to decades to be mainly the result of solar surface magnetism (Shapiro et al., 2017; Yeo et al., 2014, 2017). This is widely considered to also be the case at longer time scales of centuries and millennia (Solanki et al., 2013). The photospheric magnetic field is partially confined in kilogauss-strength magnetic concentrations, which manifest themselves as dark sunspots and bright faculae and network (Spruit & Roberts, 1983). Solar irradiance fluctuates with the changing prevalence and distribution of these bright and dark magnetic structures on the Earth-facing solar hemisphere. Based on this knowledge, historical solar irradiance is reconstructed from proxies of solar magnetism by modeling the effect of photospheric magnetism on solar irradiance (Coddington et al., 2016; Dasi-Espuig et al., 2016; Egorova et al., 2018; Shapiro et al., 2011; Steinhilber et al., 2009; Tapping et al., 2007; Wu et al., 2018).

The various reconstructions of TSI extending back to preindustrial times indicate divergent secular variability. The Maunder minimum is a solar grand minimum, a multidecade period of weak solar activity, which occurred just before the industrial revolution (around 1645 to 1715; Figure 1a). According to the CHRONOS model (Egorova et al., 2018), between the Maunder minimum and the ongoing solar activity cycle minimum, TSI rose by 3.9 to 6.3 W m^{-2} (Figure 1b). This is a recent revision of the model by Shapiro et al. (2011), which estimated a rise of 6 ± 3 W m^{-2}. The revision was prompted by the assertion by Judge et al. (2012) that Shapiro et al. (2011) might have overestimated this quantity by a factor of about 2. The other model-based estimates (Coddington et al., 2016; Dasi-Espuig et al., 2016; Steinhilber et al., 2009; Tapping et al., 2007; Wu et al., 2018) are markedly weaker and relatively consistent with one another, indicating a rise of between 0.3 and 0.9 W m^{-2} (Figure 1b). In another recent study, Lockwood and Ball (2020) concluded, from an analysis of the measurements and models of TSI over the past two solar cycles, that it cannot be excluded from the uncertainty in this data that TSI might have been 0.4 W m^{-2} lower to 0.75 W m^{-2} higher during the Maunder minimum. Furthermore, there is a claim that the last cycle minimum in 2008 might be representative of the Maunder minimum (Schrijver et al., 2011). This implies that TSI rose since the Maunder minimum by the same margin as it did since 2008, about 0.1 W m^{-2}. By current estimates, since the Maunder minimum, TSI could have risen by more than 3 W m^{-2} (Egorova et al., 2018; Judge et al., 2012; Shapiro et al., 2011) or by less than 1 W m^{-2} (Coddington et al., 2016; Dasi-Espuig et al., 2016; Steinhilber et al., 2009; Schrijver et al., 2011; Tapping et al., 2007; Wu et al., 2018) or even declined instead (Lockwood & Ball, 2020).

While there is clear evidence that greenhouse gas emissions play a significant role in global warming (Shangguan et al., 2019), quantifying its exact effects is less than straightforward due to, among other factors, the uncertainty in the secular variability in solar forcing. For certain climate models (Feulner, 2011; Fernández-Donado et al., 2013; Hind & Moberg, 2013; Luterbacher et al., 2016; Schurer et al., 2014), assuming a 3 to 6 W m^{-2} rise in TSI since the Maunder minimum produces a 0.3° C to 0.4° C greater increase in Northern Hemisphere temperatures over this period than if a rise in TSI of less than 1 W m^{-2} were considered. A steep secular rise in TSI since the Maunder minimum points to solar forcing effecting a greater temperature rise over the past centuries and hence a smaller role by greenhouse gas emissions in driving climate change. It also alludes to a greater offset to global warming by the Sun if it were to enter a grand minimum state in the future. Unfortunately, due in part to the divergence between different climate models, it remains inconclusive from climate modeling if weak or strong solar forcing is more consistent with historical temperature reconstructions (Ljungqvist et al., 2019). There is a vital need to constrain TSI secular variability more tightly and to do so in a manner that circumvents the limitations of the earlier studies, which led to the nagging uncertainty in this quantity.

To address this exigency, we make use of the recently developed, novel model of solar irradiance variability reported by Yeo et al. (2017) to constrain the rise in TSI since the Maunder minimum. The Yeo et al. (2017) model is advanced in that it is the only one reported in the literature to not require any calibration to measured solar irradiance variability. Instead of estimating the change in TSI since the Maunder minimum by reconstructing TSI back to this time, the approach and aim here are to set an upper limit by establishing the
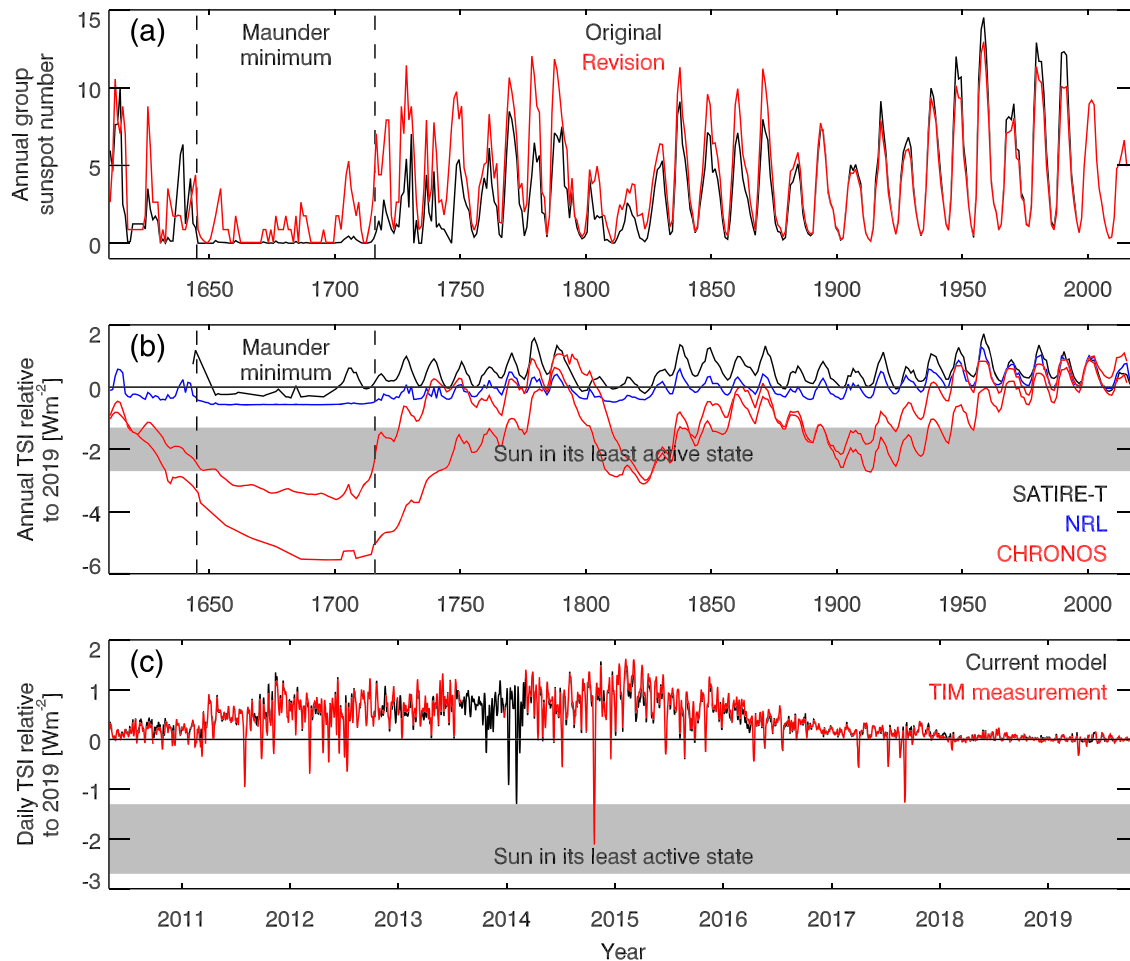
Figure 1. (a) Solar activity since the Maunder minimum, the period within the vertical dashed lines, as indicated by the group sunspot number. The original time series by Hoyt and Schatten (1998) (black) and the recent revision by Svalgaard and Schatten (2016) (red) are depicted. (b) The reconstruction of TSI over the same period from the SATIRE-T (Wu et al., 2018) (black), NRL (Coddington et al., 2016) (blue), and CHRONOS models (Egorova et al., 2018) (red), illustrating the uncertainty in the change in TSI since the Maunder minimum. (There are multiple CHRONOS TSI reconstructions, differing by the input data used. The time series indicating the weakest and strongest secular variability are depicted.) (c) The reconstruction of TSI since 2010 from the current study (black) and the measurements from SORCE/TIM (Kopp et al., 2005) (red), which monitored TSI over the same period except between August 2013 and February 2014. The root-mean-square difference between the two daily time series is 0.067 W m^{-2}, and the Pearson's correlation coefficient is 0.987; that is, the model replicates about 97% of the observed variability in the TIM record. We establish, with this model, that the TSI level of the Sun in its least-active state is 2.0 ± 0.7 W m^{-2} below the 2019 level, indicated by the shaded range in (b) and (c). Since this is the lowest level TSI can take over solar grand minima, it implies TSI could not have risen since the Maunder minimum by more than this margin, excluding the acute secular variability indicated by CHRONOS.

TSI level corresponding to the Sun in its least-active state. As this represents the lowest level TSI can take during grand solar minima, the difference to the present level represents the greatest possible rise in TSI since the Maunder minimum.

2. The Least-Active State of the Sun

Let us consider the question of what is the least-active state of the Sun. Except at the shortest and longest time scales, solar activity is dominantly driven by its magnetism. The solar magnetic field is perpetuated by global and small-scale turbulent dynamo processes. The global dynamo refers to the physical processes that produce the cyclic regeneration of the large-scale solar magnetic field that underlies the solar cycle, including the manifestation of sunspots, faculae, and network (Charbonneau, 2020). The small-scale turbulent dynamo or SSD denotes the interaction between solar convection and magnetic flux that yields the ubiquitous small-scale turbulent magnetic field on the solar surface, the so-termed internetwork magnetic field (Borrero et al., 2017). There is evidence to suggest that the internetwork magnetic field might also contribute to the magnetic network.

The dearth of sunspots during the Maunder minimum (Figure 1a) implies that the global dynamo is weak during this and other grand solar minima. At the same time, recent studies indicate that the internetwork magnetic field is unaffected by larger-scale magnetic structures (Lites, 2011; Rempel, 2014) and does not vary with the solar cycle (Buehler et al., 2013; Lites et al., 2014), implying that the SSD is not or only weakly coupled to the global dynamo. We emphasize here that while existing studies found no clear evidence that the SSD might be coupled to the global dynamo, this possibility cannot be excluded. Under the assumption that the SSD is, as the cited studies suggest, not or only weakly coupled to the global dynamo, the diminishing strength of the global dynamo over grand solar minima has limited effect on the SSD. The Sun evolves on time scales of gigayears (Sackmann et al., 1993), and the thermal relaxation time scale of the convection zone is in the order of 10^5 years (Spruit, 1982). This means the convection zone, the engine of the SSD, is in essentially the same state today as during the Maunder minimum, or indeed over the past millennia. In summary, (1) the global dynamo is weak during grand solar minima, (2) the SSD is untethered to the global dynamo and therefore unaffected by any weakening of the latter, and (3) solar convection, which drives the SSD, is invariant over the past millennia.

All considered, the scenario where the global dynamo is dormant, leaving just the SSD, represents the most inactive state the Sun can be in. In this state, there would be no sunspots or faculae due to the dormancy of the global dynamo, and the internetwork magnetic field, including the network it sustains, would extend over the entire solar surface. Assuming the SSD is, as the studies we have discussed here suggest, untethered to the global dynamo and invariant over the past millennia, the internetwork magnetic field would appear as it does today.

3. The Brightness of the Sun in Its Least-Active State

To establish the TSI level of the Sun in its least-active state, and therefore the maximum possible secular rise since the Maunder minimum, we build on the recent, groundbreaking work by Yeo et al. (2017), which presented the only reported model of solar irradiance variability to not require any calibration to measured variability. This advance, critical to our objective here, was achieved by deriving the intensity of certain solar surface features from three-dimensional (3-D) magnetohydrodynamic (MHD) simulations of the solar surface and atmosphere. Such simulations have matured to such a level of physical realism that they are able to reproduce a wide range of observational constraints (Afram et al., 2011; Danilovic et al., 2010, 2013, 2016; del Pino Alemán et al., 2018; Rempel, 2014; Riethmüller et al., 2014; Shelyag et al., 2004; Schüssler & Vögler, 2008; Yeo et al., 2017).

Other models, for simplicity, either obtain the intensity of solar surface features from semiempirical plane-parallel model solar atmospheres (Egorova et al., 2018; Dasi-Espuig et al., 2016; Shapiro et al., 2011; Wu et al., 2018) or estimate their effect on solar irradiance by the linear regression of certain indices of solar magnetism to solar irradiance measurements (Coddington et al., 2016; Steinhilber et al., 2009; Tapping et al., 2007). As a direct consequence, they feature free parameters that have to be constrained by optimizing the agreement between modeled and measured solar irradiance variability. This renders the model output, including the reconstructed secular variability, susceptible to the uncertainty in solar irradiance measurements. This is compounded by the fact that the linear regression of indices of solar magnetism to solar irradiance measurements is a crude simplification of the nuanced relationship between solar surface magnetism and irradiance variability (Yeo et al., 2014; Yeo & Krivova, 2019). Also, plane-parallel model atmospheres, the one-dimensional simplification of the spatially inhomogeneous solar atmosphere, cannot capture all the relevant physics (Holzreuter & Solanki, 2013; Uitenbroek & Criscuoli, 2011).

In an advance, the 3-D MHD simulations-based model presented by Yeo et al. (2017) reproduces measured TSI variability without any of these simplifications or calibration to the latter. The model does, however, make the assumption that the solar surface outside of sunspots, faculae, and network (i.e., the internetwork) is field-free, neglecting the SSD and the internetwork magnetic field it maintains. The results of recent simulations (Rempel, 2020), indicating that the brightness of the internetwork changes with the strength of the internetwork magnetic field, suggest that this assumption might be problematic. In this study, we extend the Yeo et al. (2017) model to include a physically realistic description of the internetwork by using an updated

3-D MHD code to generate simulations of the SSD. This not only renders the model even more physical but, critically, also enables us to compute the TSI level of the Sun in its least-active state, where the global dynamo is dormant, leaving just the SSD active (section 2). And the unique strength of the Yeo et al. (2017) approach allows us to do so while circumventing the limitations of other models, which contributed to the gross uncertainty in TSI secular variability.

Based on the assumption that the variation in TSI at time scales greater than a day is dominantly driven by solar surface magnetism, the Yeo et al. (2017) model describes the variation in TSI due to the changing prevalence and distribution of bright and dark magnetic structures on the solar disc. The model has two inputs. The first is the solar disc coverage by magnetic features. These come in the form of faculae and network, classed together and termed collectively as faculae, and of sunspots. The disc coverage by faculae and sunspots is derived by identifying these solar surface features in full-disc longitudinal magnetograms and continuum intensity images from the HMI instrument onboard the SDO mission, launched in 2010 (Scherrer et al., 2012). The solar disc outside of sunspots and faculae (including network) is taken to be the internetwork. The second input is the emergent intensity from sunspots, faculae, and the internetwork. Sunspot intensity is calculated from plane-parallel model atmospheres (Unruh et al., 1999) and facular and internetwork intensity from 3-D model atmospheres using radiative transfer codes. Sunspots can be reasonably well represented by plane-parallel model atmospheres such that their application to the model reproduces the effect of sunspots on TSI while maintaining its independence from calibration to measured solar irradiance variability. The 3-D model atmospheres are based on MHD simulations of facular and internetwork regions executed with the MURaM code (Rempel, 2014, 2020; Vögler & Schüssler, 2007). Importantly, while Yeo et al. (2017) had represented the internetwork with field-free simulations, neglecting the SSD and the internetwork magnetic field, we make use of a more recent version of the MURaM code than was used in this earlier study to generate simulations that emulate SSD action and replicate the internetwork magnetic field.

There are four simulation runs (Figure 2a), set up to emulate SSD action (Rempel, 2014, 2020; Vögler & Schüssler, 2007). The first run, representing the internetwork, is initiated with a weak, random magnetic field (root-mean-square field strength of 10^{-3} G). This seed field is amplified and reorganized in the simulation into a small-scale turbulent field resembling the internetwork magnetic field. The other three runs, representing facular regions with varying levels of magnetic flux, were initiated with a uniform vertical magnetic field of 100, 200, and 300 G, respectively. As in the first run, these runs emulate SSD action and replicate the internetwork magnetic field. However, having imposed net magnetic flux, these runs also form kilogauss-strength magnetic aggregations in the intergranular lanes, that is, network and faculae-like features. Ten samples are taken of each run, and the emergent intensity from each simulation snapshot, essentially a 3-D model atmosphere, is computed (Figure 2b). Internetwork intensity is given by the mean intensity of the SSD-only run snapshots, and facular intensity by the intensity of the facular features apparent in the snapshots of the facular runs. MURaM simulations are well suited for the current purpose, having been demonstrated in multiple studies to reproduce the observed properties of the internetwork magnetic field (Danilovic et al., 2010, 2016; del Pino Alemán et al., 2018; Rempel, 2014; Schüssler & Vögler, 2008) and of faculae and network (Afram et al., 2011; Danilovic et al., 2013; Riethmüller et al., 2014; Shelyag et al., 2004; Yeo et al., 2017).

Given the surface coverage by sunspots and faculae at a particular time, the model computes the corresponding TSI level by assigning to each point on the solar disc the appropriate intensity depending on whether it is in a sunspot, in faculae, or the internetwork. Using an HMI longitudinal magnetogram and the concurrent continuum intensity image from each day between 30 April 2010, when the instrument started regular operation, and 31 December 2019 as input into our TSI model, we reconstruct the daily TSI over the intervening period (Figure 1c). The reconstruction closely reproduces measured TSI variability. The Sun is at its least active when the global dynamo is dormant and the internetwork magnetic field maintained by the SSD extends over the entire solar surface (section 2). And since the SSD is likely untethered to the global dynamo and invariant over the past millennia, the TSI level of the Sun in this state emerges from the model by taking the entire solar disc to resemble the present-day internetwork. The absolute scale of the model is set to that of the SORCE/TIM TSI record (Kopp et al., 2005), the radiometry of which is widely regarded to be the most reliable (Fehlmann et al., 2012). To this end, we normalize the reconstruction of daily TSI over the last decade to the TIM record and apply the same normalization factor to the TSI level of the Sun in its
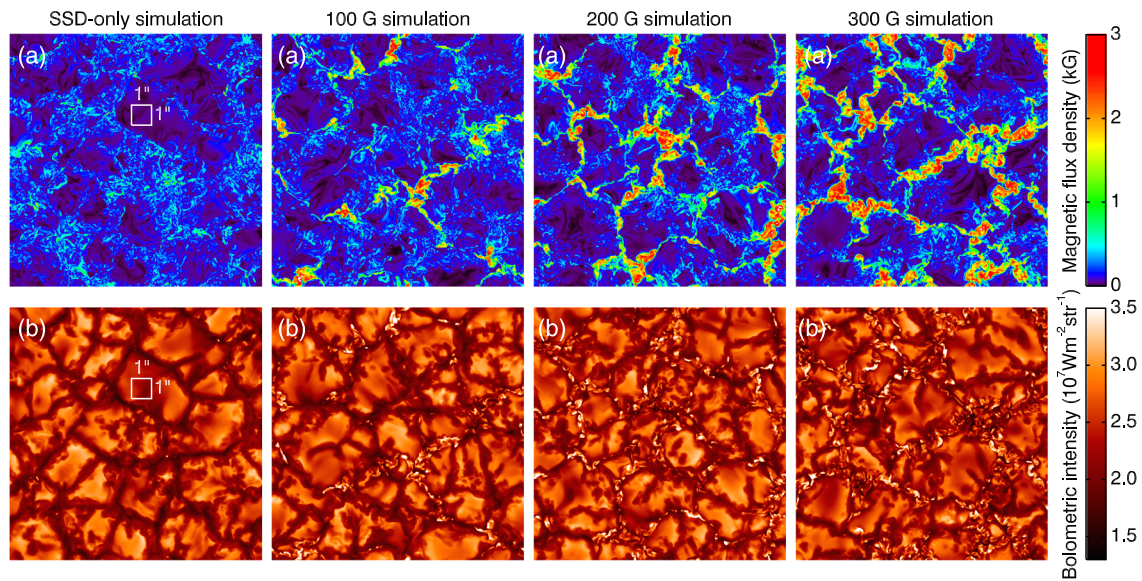
Figure 2. Three-dimensional MHD simulations of the solar surface and atmosphere and the calculated emergent intensity. (a) Magnetic flux density at optical depth unity (i.e., at the solar surface) in a snapshot of each simulation run and (b) the corresponding bolometric image, calculated from each snapshot using a radiative transfer code. The simulation runs are set up to emulate the small-scale turbulent dynamo, producing the ubiquitous small-scale turbulent magnetic field. Into three of the four runs, a uniform vertical magnetic field of 100, 200, and 300 G was introduced. After these simulations reached statistical equilibrium, the imposed net magnetic flux aggregates in the intergranular lanes, forming the kilogauss-strength magnetic concentrations apparent as comparatively small bright features in the bolometric images. The white box in the left column denotes 1×1 arcsec, corresponding to an area of approximately 725×725 km on the Sun.

least-active state, arriving at the final value of $1{,}358.7 \pm 0.7$ W m^{-2} (shaded range, Figures 1b and 1c). We emphasize that this normalization merely sets the absolute scale of the model to that of the TIM record; the TSI level of the Sun in its least-active state relative to the present level is unaffected. The associated error, 0.7 W m^{-2}, denotes the uncertainty in this quantity from the uncertainty in the simulation of the internetwork magnetic field. This is a conservative estimate derived by repeating the above analysis for the extreme scenario that the internetwork is field free.

Since the TSI level of the least-active Sun, $1{,}358.7 \pm 0.7$ W m^{-2} is the lowest level TSI can take during grand solar minima, the difference to the 2019 level, 2.0 ± 0.7 W m^{-2} (shaded range, Figures 1b and 1c), represents the maximum possible rise in TSI since the Maunder minimum. The TSI model and the above analysis are further detailed in the supporting information.

The occurrence of numerous and/or sizable sunspots can produce large dips in TSI, even below the level of the least-active Sun, $1{,}358.7 \pm 0.7$ W m^{-2}, such as in October 2014 (Figure 1c). It is unlikely, however, that sunspots might have suppressed the secular trend in TSI over the Maunder minimum below this level. First, there was a dearth of sunspots during the Maunder minimum (Figure 1a). Second, darkening by a sunspot is a short-term phenomenon and not a state the Sun can sustain over the duration of a solar cycle, much less a grand minimum.

4. Comparison to Other Estimates of the Change in TSI Since the Maunder Minimum

The cap on the rise in TSI since the Maunder minimum derived here, 2.0 ± 0.7 W m^{-2}, encloses all the current estimates (Coddington et al., 2016; Dasi-Espuig et al., 2016; Egorova et al., 2018; Judge et al., 2012; Lockwood & Ball, 2020; Schrijver et al., 2011; Shapiro et al., 2011; Steinhilber et al., 2009; Tapping et al., 2007; Wu et al., 2018) except the range of 3 to 6.3 W m^{-2} indicated by Shapiro et al. (2011), the reassessment of their model by Judge et al. (2012), and CHRONOS (Egorova et al., 2018) (Figure 1b). We consider the upper limit established here to be more reliable than the existing estimates. As argued in section 3, the Yeo et al. (2017) modeling approach circumvents the limitations of the simpler models employed in the earlier works. And as we will argue next, the model atmospheres employed by Shapiro et al. (2011) and CHRONOS are ill-suited for estimating TSI secular variability via their methodology. In these two models, the intensity of the quiet

Sun is assumed to vary with solar activity between two defined limits, and this forms the main contribution to the reconstructed secular variability. (The quiet Sun refers to the solar surface outside of sunspots and faculae, i.e., network and internetwork.) In Shapiro et al. (2011), the lower and upper limits are given by the FAL-A and FAL-C plane-parallel model solar atmospheres (Fontenla et al., 1999), respectively. The FAL-A and FAL-C models correspond to quiet Sun regions with different amounts of magnetic flux and therefore different intensities. Judge et al. (2012) raised questions over the use of the FAL-A model as the lower limit, leading CHRONOS to employ an amalgamation of the FAL-A and FAL-C models, termed PW-B, as the lower limit instead (Egorova et al., 2018).

The FAL model atmospheres are, however, not designed for their intended purpose in Shapiro et al. (2011) and CHRONOS. As noted earlier, plane-parallel representations of the spatially inhomogeneous solar atmosphere cannot capture all the relevant physics. Multiple studies demonstrated that plane-parallel model atmospheres cannot fully return the true average intensity spectra of the regions they represent (Holzreuter & Solanki, 2013; Uitenbroek & Criscuoli, 2011). More critically, while solar electromagnetic radiation and consequently TSI variability are produced mainly in the photosphere, the photospheric layers of the FAL model atmospheres, and therefore also those of PW-B, are poorly constrained (Vernazza et al., 1981). This is due to the fact that the FAL model atmospheres are based on ultraviolet measurements formed largely in the chromosphere. As an example, if the PW-B model were to be made a mere 10 K warmer, a margin smaller than the accuracy of this and other such model atmospheres, CHRONOS TSI secular variability would decrease by a factor of about 5 (see the supporting information). Consequently, the FAL models are not accurate enough to support the acute TSI secular variability indicated by Shapiro et al. (2011) and CHRONOS. The approach taken here, by relying on 3-D model atmospheres based on realistic simulations of the solar surface and atmosphere that reproduces a wide range of photospheric observational constraints (Afram et al., 2011; Danilovic et al., 2010, 2013, 2016; del Pino Alemán et al., 2018; Rempel, 2014; Riethmüller et al., 2014; Shelyag et al., 2004; Schüssler & Vögler, 2008; Yeo et al., 2017), circumvents these limitations.

5. Conclusion

There is significant uncertainty in the historical secular variability in solar irradiance, with current estimates of the change in TSI since the Maunder minimum ranging from a drop of 0.75 W m^{-2} to a rise of 6.3 W m^{-2}. This in turn introduces considerable uncertainty in the contribution of the Sun to climate change. By demonstrating that the Sun in its least-active state is at the most 2.0±0.7 W m^{-2} dimmer than it was over 2019, we greatly constrain the change in TSI since the Maunder minimum by ruling out rises above this margin. This constraint on TSI secular variability over the past centuries, by limiting the possible contribution by solar forcing to global temperature changes, will be a boon to the climate change assessment.

Acronyms

3-D	three dimensional
CHRONOS	Code for the High spectral ResolutiOn recoNstructiOn of Solar irradiance
FAL-A	Fontenla, Avrett, and Loeser Model A
FAL-C	Fontenla, Avrett, and Loeser Model C
HMI	Helioseismic and Magnetic Imager
IPCC	Intergovernmental Panel on Climate Change
MHD	magnetohydrodynamic
MURaM	Max Planck Institute for Solar System Research and University of Chicago Radiation MHD code
NRL	Naval Research Laboratory
PW-B	present work Model B
SATIRE-T	Spectral And Total Irradiance REconstruction for the Telescope era
SDO	Solar Dynamics Observatory
SORCE	SOlar Radiation and Climate Experiment
SSD	small-scale dynamo
TIM	total irradiance monitor
TSI	total solar irradiance

Conflict of Interest

We declare that none of the authors have any competing interests.

Data Availability Statement

The group sunspot number record is available online (at www.sidc.be/silso/groupnumberv3), and the SORCE/TIM TSI record is available at the LISIRD website (at lasp.colorado.edu/lisird/). The TSI model makes use of solar imagery from the NASA SDO mission (available at jsoc.stanford.edu). The model output TSI reconstruction is available online (at www2.mps.mpg.de/projects/sun-climate/data.html).

References

Afram, N., Unruh, Y. C., Solanki, S. K., Schüssler, M., Lagg, A., & Vögler, A. (2011). Intensity contrast from MHD simulations and HINODE observations. *Astronomy & Astrophysics*, *526*, A120. https://doi.org/10.1051/0004-6361/201015582

Borrero, J. M., Jafarzadeh, S., Schüssler, M., & Solanki, S. K. (2017). Solar magnetoconvection and small-scale dynamo. Recent Developments in Observation and Simulation. *Space Science Reviews*, *210*(1–4), 275–316. https://doi.org/10.1007/s11214-015-0204-5

Buehler, D., Lagg, A., & Solanki, S. K. (2013). Quiet Sun magnetic fields observed by Hinode: Support for a local dynamo. *Astronomy & Astrophysics*, *555*, A33. https://doi.org/10.1051/0004-6361/201321152

Charbonneau, P. (2020). Dynamo models of the solar cycle. *Living Reviews in Solar Physics*, *17*(1), 4. https://doi.org/10.1007/s41116-020-00025-6

Coddington, O., Lean, J. L., Pilewskie, P., Snow, M., & Lindholm, D. (2016). A solar irradiance climate data record. *Bulletin of the American Meteorological Society*, *97*(7), 1265. https://doi.org/10.1175/BAMS-D-14-00265.1

Danilovic, S., Röhrbein, D., Cameron, R. H., & Schüssler, M. (2013). On the relation between continuum brightness and magnetic field in solar active regions. *Astronomy & Astrophysics*, *550*, A118. https://doi.org/10.1051/0004-6361/201219726

Danilovic, S., Rempel, M., van Noort, M., & Cameron, R. (2016). Observed and simulated power spectra of kinetic and magnetic energy retrieved with 2D inversions. *Astronomy & Astrophysics*, *594*, A103. https://doi.org/10.1051/0004-6361/201527917

Danilovic, S., Schüssler, M., & Solanki, S. K. (2010). Probing quiet Sun magnetism using MURaM simulations and Hinode/SP results: Support for a local dynamo. *Astronomy & Astrophysics*, *513*, A1. https://doi.org/10.1051/0004-6361/200913379

Dasi-Espuig, M., Jiang, J., Krivova, N. A., Solanki, S. K., Unruh, Y. C., & Yeo, K. L. (2016). Reconstruction of spectral solar irradiance since 1700 from simulated magnetograms. *Astronomy & Astrophysics*, *590*, A63. https://doi.org/10.1051/0004-6361/201527993

del Pino Alemán, T., Trujillo Bueno, J., Štěpán, J., & Shchukina, N. (2018). A novel investigation of the small-scale magnetic activity of the quiet Sun via the Hanle effect in the Sr I 4607 Å line. *The Astrophysical Journal*, *863*(2), 164. https://doi.org/10.3847/1538-4357/aaceab

Egorova, T., Schmutz, W., Rozanov, E., Shapiro, A. I., Usoskin, I., Beer, J., et al. (2018). Revised historical solar irradiance forcing. *Astronomy & Astrophysics*, *615*, A85. https://doi.org/10.1051/0004-6361/201731199

Fehlmann, A., Kopp, G., Schmutz, W., Winkler, R., Finsterle, W., & Fox, N. (2012). Fourth world radiometric reference to SI radiometric scale comparison and implications for on-orbit measurements of the total solar irradiance. *Metrologia*, *49*(2), S34–S38. https://doi.org/10.1088/0026-1394/49/2/S34

Fernández-Donado, L., González-Rouco, J. F., Raible, C. C., Ammann, C. M., Barriopedro, D., García-Bustamante, E., et al. (2013). Large-scale temperature response to external forcing in simulations and reconstructions of the last millennium. *Climate of the Past*, *9*(1), 393–421. https://doi.org/10.5194/cp-9-393-2013

Feulner, G. (2011). Are the most recent estimates for Maunder minimum solar irradiance in agreement with temperature reconstructions? *Geophysical Research Letters*, *38*, L16706. https://doi.org/10.1029/2011GL048529

Fontenla, J., White, O. R., Fox, P. A., Avrett, E. H., & Kurucz, R. L. (1999). Calculation of solar irradiances. I. Synthesis of the solar spectrum. *The Astrophysical Journal*, *518*(1), 480–499. https://doi.org/10.1086/307258

Gray, L. J., Beer, J., Geller, M., Haigh, J. D., Lockwood, M., Matthes, K., et al. (2010). Solar influences on climate. *Reviews of Geophysics*, *48*, RG4001. https://doi.org/10.1029/2009RG000282

Hind, A., & Moberg, A. (2013). Past millennial solar forcing magnitude. *Climate Dynamics*, *41*(9–10), 2527–2537. https://doi.org/10.1007/s00382-012-1526-6

Holzreuter, R., & Solanki, S. K. (2013). Three-dimensional non-LTE radiative transfer effects in Fe i lines. II. Line formation in 3D radiation hydrodynamic simulations. *Astronomy & Astrophysics*, *558*, A20. https://doi.org/10.1051/0004-6361/201322135

Hoyt, D. V., & Schatten, K. H. (1998). Group sunspot numbers: A new solar activity reconstruction. *Solar Physics*, *181*(2), 491–512. https://doi.org/10.1023/A:1005056326158

IPCC (2013). *Climate change 2013: The Physical Science Basis. Contribution of Working Group I to the Fifth Assessment Report of the Intergovernmental Panel on Climate Change*, In T. F. Stocker (Eds.),. et al. Cambridge, United Kingdom and New York, NY, USA: Cambridge University Press. https://doi.org/10.1017/CBO9781107415324

IPCC (2018). Global Warming of 1.5 C. An IPCC Special Report on the impacts of global warming of 1.5° C above pre-industrial levels and related global greenhouse gas emission pathways, in the context of strengthening the global response to the threat of climate change, sustainable development, and efforts to eradicate poverty. www.ipcc.ch/sr15 In press.

Judge, P. G., Lockwood, G. W., Radick, R. R., Henry, G. W., Shapiro, A. I., Schmutz, W., & Lindsey, C. (2012). Confronting a solar irradiance reconstruction with solar and stellar data. *Astronomy & Astrophysics*, *544*, A88. https://doi.org/10.1051/0004-6361/201218903

Kopp, G. (2014). An assessment of the solar irradiance record for climate studies. *Journal of Space Weather and Space Climate*, *4*, A14. https://doi.org/10.1051/swsc/2014012

Kopp, G., Lawrence, G., & Rottman, G. (2005). The Total Irradiance Monitor (TIM): Science results. *Solar Physics*, *230*(1–2), 129–139. https://doi.org/10.1007/s11207-005-7433-9

Lites, B. W. (2011). Hinode observations suggesting the presence of a local small-scale turbulent dynamo. *The Astrophysical Journal*, *737*(2), 52. https://doi.org/10.1088/0004-637X/737/2/52

Lites, B. W., Centeno, R., & McIntosh, S. W. (2014). The solar cycle dependence of the weak internetwork flux. *Publications of the Astronomical Society of Japan*, *66*, S4. https://doi.org/10.1093/pasj/psu082

Ljungqvist, F. C., Zhang, Q., Brattström, G., Krusic, P. J., Seim, A., Li, Q., et al. (2019). Centennial-scale temperature change in last millennium simulations and proxy-based reconstructions. *Journal of Climate*, *32*(9), 2441–2482. https://doi.org/10.1175/JCLI-D-18-0525.1

Lockwood, M., & Ball, W. T. (2020). Placing limits on long-term variations in quiet-Sun irradiance and their contribution to total solar irradiance and solar radiative forcing of climate. *Proceedings of the Royal Society A*, *476*(2238), 20200077. https://doi.org/10.1098/rspa.2020.0077

Luterbacher, J., Werner, J. P., Smerdon, J. E., Fernández-Donado, L., González-Rouco, F. J., Barriopedro, D., et al. (2016). European summer temperatures since Roman times. *Environmental Research Letters*, *11*(2), 024001. https://doi.org/10.1088/1748-9326/11/2/024001

Rempel, M. (2014). Numerical simulations of quiet Sun magnetism: On the contribution from a small-scale dynamo. *The Astrophysical Journal*, *789*(2), 132. https://doi.org/10.1088/0004-637X/789/2/132

Rempel, M. (2020). On the contribution of quiet-Sun magnetism to solar irradiance variations: Constraints on quiet-Sun variability and grand-minimum scenarios. *The Astrophysical Journal*, *894*(2), 140. https://doi.org/10.3847/1538-4357/ab8633

Riethmüller, T. L., Solanki, S. K., Berdyugina, S. V., Schüssler, M., Martínez Pillet, V., Feller, A., et al. (2014). Comparison of solar photospheric bright points between Sunrise observations and MHD simulations. *Astronomy & Astrophysics*, *568*, A13. https://doi.org/10.1051/0004-6361/201423892

Sackmann, I. J., Boothroyd, A. I., & Kraemer, K. E. (1993). Our Sun. III. Present and future. *The Astrophysical Journal*, *418*, 457. https://doi.org/10.1086/173407

Schüssler, M., & Vögler, A. (2008). Strong horizontal photospheric magnetic field in a surface dynamo simulation. *Astronomy & Astrophysics*, *481*(1), L5–L8. https://doi.org/10.1051/0004-6361:20078998

Scherrer, P. H., Schou, J., Bush, R. I., Kosovichev, A. G., Bogart, R. S., Hoeksema, J. T., et al. (2012). The Helioseismic and Magnetic Imager (HMI) Investigation for the Solar Dynamics Observatory (SDO). *Solar Physics*, *275*(1–2), 207–227. https://doi.org/10.1007/s11207-011-9834-2

Schrijver, C. J., Livingston, W. C., Woods, T. N., & Mewaldt, R. A. (2011). The minimal solar activity in 2008–2009 and its implications for long-term climate modeling. *Geophysical Research Letters*, *38*, L06701. https://doi.org/10.1029/2011GL046658

Schurer, A. P., Tett, S. F. B., & Hegerl, G. C. (2014). Small influence of solar variability on climate over the past millennium. *Nature Geoscience*, *7*(2), 104–108. https://doi.org/10.1038/ngeo2040

Shangguan, M., Wang, W., & Jin, S. (2019). Variability of temperature and ozone in the upper troposphere and lower stratosphere from multi-satellite observations and reanalysis data. *Atmospheric Chemistry and Physics*, *19*(10), 6659–6679. https://acp.copernicus.org/articles/19/6659/2019/

Shapiro, A. I., Schmutz, W., Rozanov, E., Schoell, M., Haberreiter, M., Shapiro, A. V., & Nyeki, S. (2011). A new approach to the long-term reconstruction of the solar irradiance leads to large historical solar forcing. *Astronomy & Astrophysics*, *529*, A67. https://doi.org/10.1051/0004-6361/201016173

Shapiro, A. I., Solanki, S. K., Krivova, N. A., Cameron, R. H., Yeo, K. L., & Schmutz, W. K. (2017). The nature of solar brightness variations. *Nature Astronomy*, *1*, 612–616. https://doi.org/10.1038/s41550-017-0217-y

Shelyag, S., Schüssler, M., Solanki, S. K., Berdyugina, S. V., & Vögler, A. (2004). G-band spectral synthesis and diagnostics of simulated solar magneto-convection. *Astronomy & Astrophysics*, *427*, 335–343. https://doi.org/10.1051/0004-6361:20040471

Solanki, S. K., Krivova, N. A., & Haigh, J. D. (2013). Solar irradiance variability and climate. *Annual Review of Astronomy and Astrophysics*, *51*(1), 311–351. https://doi.org/10.1146/annurev-astro-082812-141007

Spruit, H. C. (1982). Effect of spots on a star's radius and luminosity. *Astronomy & Astrophysics*, *108*(2), 348–355.

Spruit, H. C., & Roberts, B. (1983). Magnetic flux tubes on the Sun. *Nature*, *304*(5925), 401–406. https://doi.org/10.1038/304401a0

Steinhilber, F., Beer, J., & Fröhlich, C. (2009). Total solar irradiance during the Holocene. *Geophysical Research Letters*, *36*, L19704. https://doi.org/10.1029/2009GL040142

Svalgaard, L., & Schatten, K. H. (2016). Reconstruction of the sunspot group number: The backbone method. *Solar Physics*, *291*(9–10), 2653–2684. https://doi.org/10.1007/s11207-015-0815-8

Tapping, K. F., Boteler, D., Charbonneau, P., Crouch, A., Manson, A., & Paquette, H. (2007). Solar magnetic activity and total irradiance since the Maunder minimum. *Solar Physics*, *246*(2), 309–326. https://doi.org/10.1007/s11207-007-9047-x

Uitenbroek, H., & Criscuoli, S. (2011). Why one-dimensional models fail in the diagnosis of average spectra from inhomogeneous stellar atmospheres. *The Astrophysical Journal*, *736*(1), 69. https://doi.org/10.1088/0004-637X/736/1/69

Unruh, Y. C., Solanki, S. K., & Fligge, M. (1999). The spectral dependence of facular contrast and solar irradiance variations. *Astronomy & Astrophysics*, *345*, 635–642.

Vögler, A., & Schüssler, M. (2007). A solar surface dynamo. *Astronomy & Astrophysics*, *465*(3), L43–L46. https://doi.org/10.1051/0004-6361:20077253

Vernazza, J. E., Avrett, E. H., & Loeser, R. (1981). Structure of the solar chromosphere. III. Models of the EUV brightness components of the quiet Sun. *The Astrophysical Journal Supplement Series*, *45*, 635–725. https://doi.org/10.1086/190731

Wu, C. J., Krivova, N. A., Solanki, S. K., & Usoskin, I. G. (2018). Solar total and spectral irradiance reconstruction over the last 9000 years. *Astronomy & Astrophysics*, *620*, A120. https://doi.org/10.1051/0004-6361/201832956

Yeo, K. L., & Krivova, N. A. (2019). Intensity contrast of solar network and faculae. II. Implications for solar irradiance modelling. *Astronomy & Astrophysics*, *624*, A135. https://doi.org/10.1051/0004-6361/201935123

Yeo, K. L., Krivova, N. A., & Solanki, S. K. (2014). Solar cycle variation in solar irradiance. *Space Science Reviews*, *186*(1–4), 137–167. https://doi.org/10.1007/s11214-014-0061-7

Yeo, K. L., Krivova, N. A., Solanki, S. K., & Glassmeier, K. H. (2014). Reconstruction of total and spectral solar irradiance from 1974 to 2013 based on KPVT, SoHO/MDI, and SDO/HMI observations. *Astronomy & Astrophysics*, *570*, A85. https://doi.org/10.1051/0004-6361/201423628

Yeo, K. L., Solanki, S. K., Norris, C. M., Beeck, B., Unruh, Y. C., & Krivova, N. A. (2017). Solar irradiance variability is caused by the magnetic activity on the solar surface. *Physical Reviews Letters*, *119*, 091102. https://doi.org/10.1103/PhysRevLett.119.091102